Experimental Section

Synthesis of FsGDY/Fe_2O_3 Composite

According to literature procedures, the monomer was synthesized starting from 1,3,5-trifluorobenzene. Sequential bromination and Sonogashira cross-coupling reactions were employed to introduce trimethylsilyl (TMS) protecting groups, successfully affording the intermediate 1,3,5-tris((trimethylsilyl)ethynyl)-2,4,6-trifluorobenzene.[1]

Under an argon atmosphere, the intermediate 1,3,5-tris((trimethylsilyl)ethynyl)-2,4,6-trifluorobenzene (247 mg) was dissolved in 40 mL of anhydrous tetrahydrofuran (THF). The reaction system was then cooled to a low temperature using a liquid nitrogen bath. While maintaining low temperature and continuous stirring, a solution of tetra-n-butylammonium fluoride (TBAF, 2.94 mL, 1 M in THF) was slowly added via syringe. After complete addition, the reaction was maintained at low temperature for 10 minutes. Upon completion, 30 mL of ethyl acetate was added to the mixture for extraction and dilution. The combined solution was transferred to a separatory funnel and thoroughly washed with saturated brine (30 mL × 3) to remove water-soluble by-products such as the tetra-n-butylammonium salts generated during the reaction. The separated organic phase was dried over anhydrous sodium sulfate, filtered, and concentrated via rotary evaporation to remove the solvent, yielding the final target product: 1,3,5-triethynyl-2,4,6-trifluorobenzene.

The obtained monomer (approximately 120 mg), 50 g of anhydrous ferric chloride ($FeCl_3$), and 10 g of anhydrous copper(II) acetate ($Cu(OAc)_2$) were thoroughly ground and mixed uniformly, then placed in a reaction autoclave. The reaction proceeded at 110 °C for 12 hours. After the reaction, the mixture was repeatedly washed with deionized water to completely remove the molten salt medium. The resulting solid was freeze-dried and subsequently calcined at 300 °C for 2 hours in a muffle furnace, ultimately yielding a reddish-brown FsGDY/Fe_2O_3 composite nanomaterial.

Materials Characterization

Morphological details were examined by field-emission scanning electron microscopy (FE-SEM, Hitachi SU8600) and field-emission transmission electron microscopy (FE-TEM, JEOL JEM-2100PLUS). The chemical structure of the product was characterized by Fourier transform infrared spectroscopy (FT-IR, Nicolet IS10) and Raman spectroscopy (Renishaw inVia, 532 nm excitation). Crystal structure and phase purity were analyzed by X-ray diffraction (XRD) on a Rigaku ULTIMA IV diffractometer using Cu Kα radiation (λ = 1.5418 Å) operated at 40 kV and 40 mA. The surface chemical composition and valence states were investigated by X-ray photoelectron spectroscopy (XPS) on a Thermo Scientific ESCALAB Xi+ spectrometer using a monochromatic Al Kα X-ray source. Thermal stability was evaluated by thermogravimetric analysis (TGA) on a NETZSCH TG 209 F1 Libra instrument. Measurements were performed from room temperature to 800 °C under an air atmosphere at a heating rate of 10 °C min^{-1}. Nitrogen adsorption-desorption measurements were conducted at 77 K using a Micromeritics ASAP2460 gas

adsorption system. UV-Vis absorption spectra were acquired on an Agilent Cary 5000 spectrometer.

Electrochemical Measurements

The working electrode was fabricated by mixing the active material (FsGDY/Fe_2O_3 composite), conductive agent (carbon black), and binder (polyvinylidene fluoride, PVDF) in a mass ratio of 7:2:1. The binder was a 2.5 wt% PVDF solution pre-dissolved in N-methyl-2-pyrrolidone (NMP) solvent. The mixture was thoroughly ground to form a homogeneous slurry, which was then coated onto a copper foil current collector and vacuum-dried at 80 °C for 12 hours. The resulting electrode film was punched into circular discs with a diameter of 12 mm for use. The mass loading of the active material on the prepared electrode was calculated to be approximately 0.6 mg cm^{-2}.

CR2032 coin-type half-cells were assembled in an argon-filled glove box, using lithium foil as the counter electrode and Celgard 2500 as the separator. The electrolyte consisted of 1 M $LiPF_6$ dissolved in a mixture of ethylene carbonate (EC) and dimethyl carbonate (DMC) (1:1 by volume), with a 5% addition of fluoroethylene carbonate (FEC). The assembled cells were cycled between 0.005 and 3 V using a LAND battery test system. Electrochemical impedance spectroscopy (EIS) measurements were performed on a ZAHNER ZENNIUM electrochemical workstation at room temperature by applying an AC voltage with an amplitude of 5 mV.

Supporting Figures

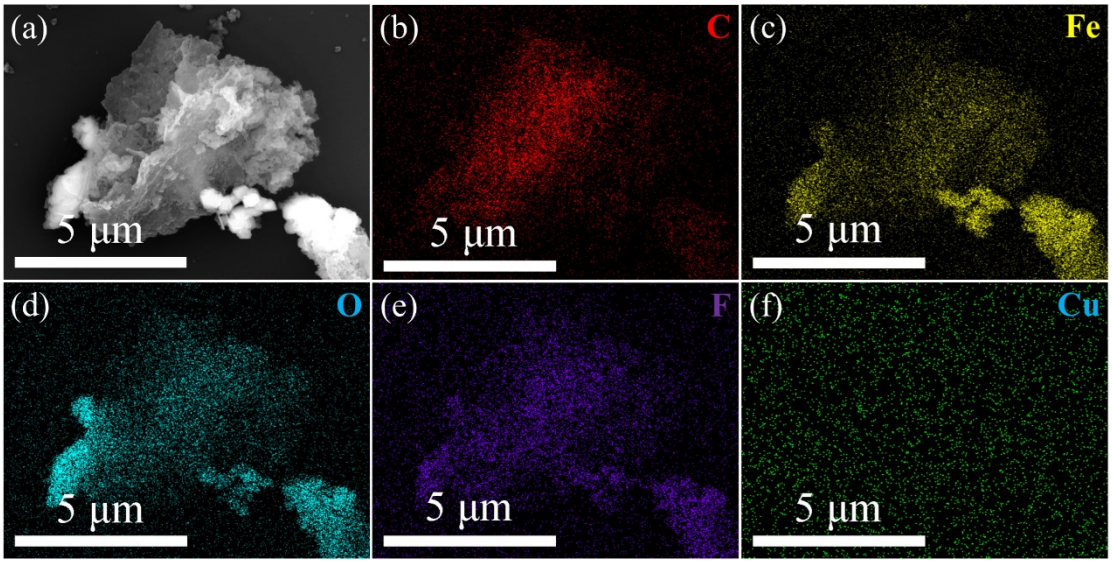

Fig. S1 (a-f) The SEM images and element mapping images of C, Fe, O, F, and Cu, respectively.

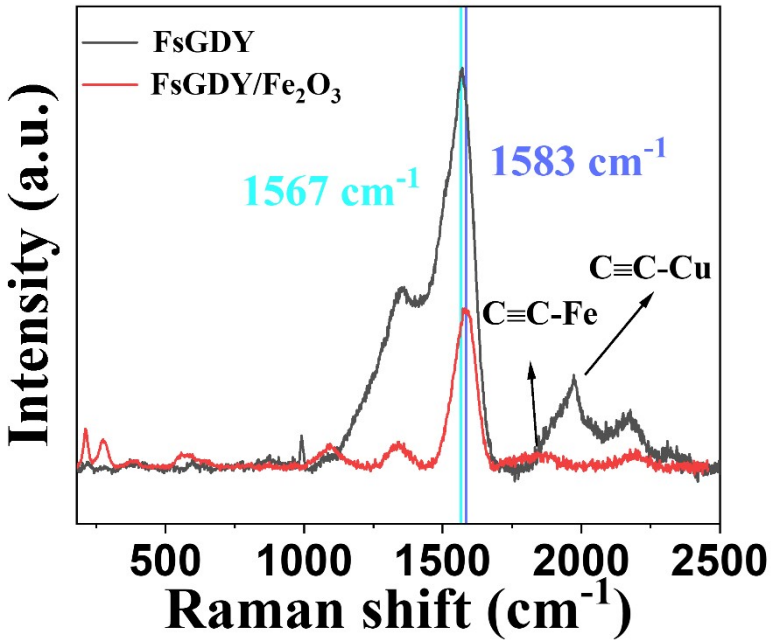

Fig. S2 Raman comparison of FsGDY and FsGDY/Fe_2O_3.

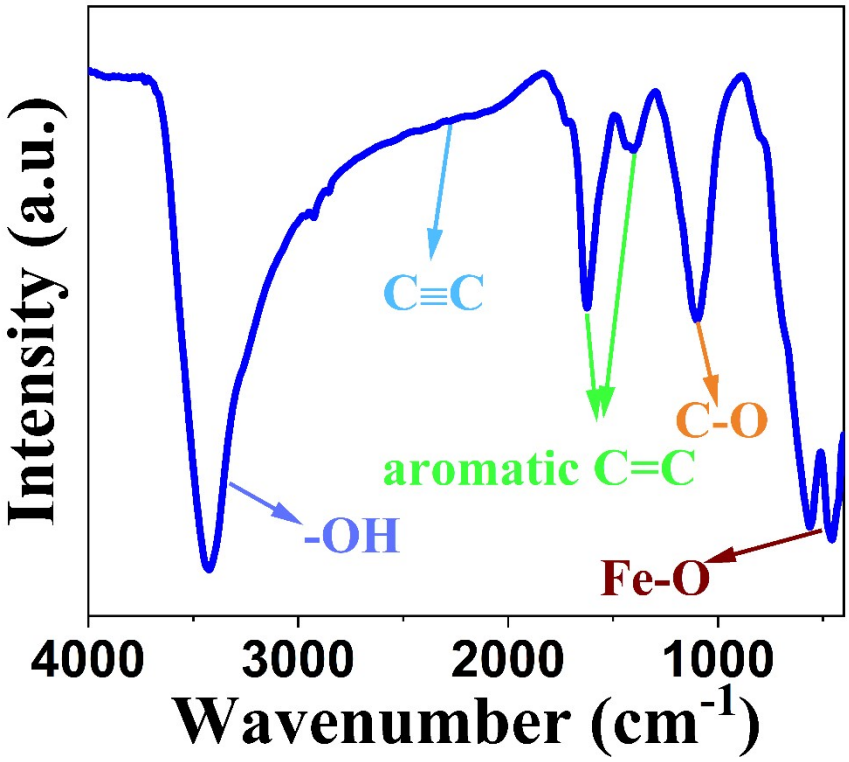

Fig. S3 FT-IR spectrum of FsGDY/Fe_2O_3 composite.

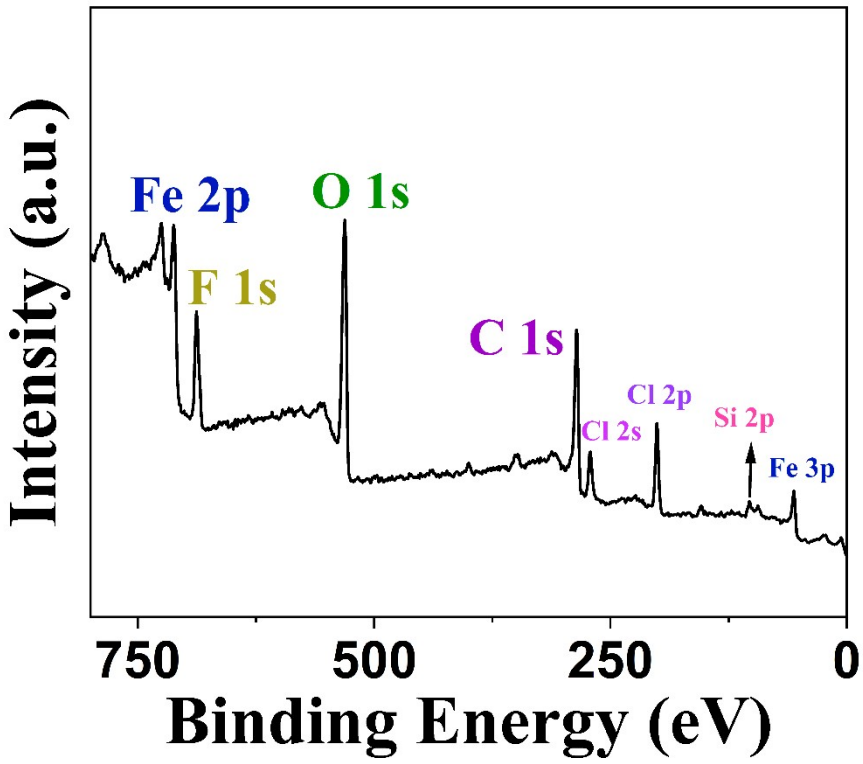

Fig. S4 High-resolution XPS spectra of FsGDY/Fe_2O_3 composite.

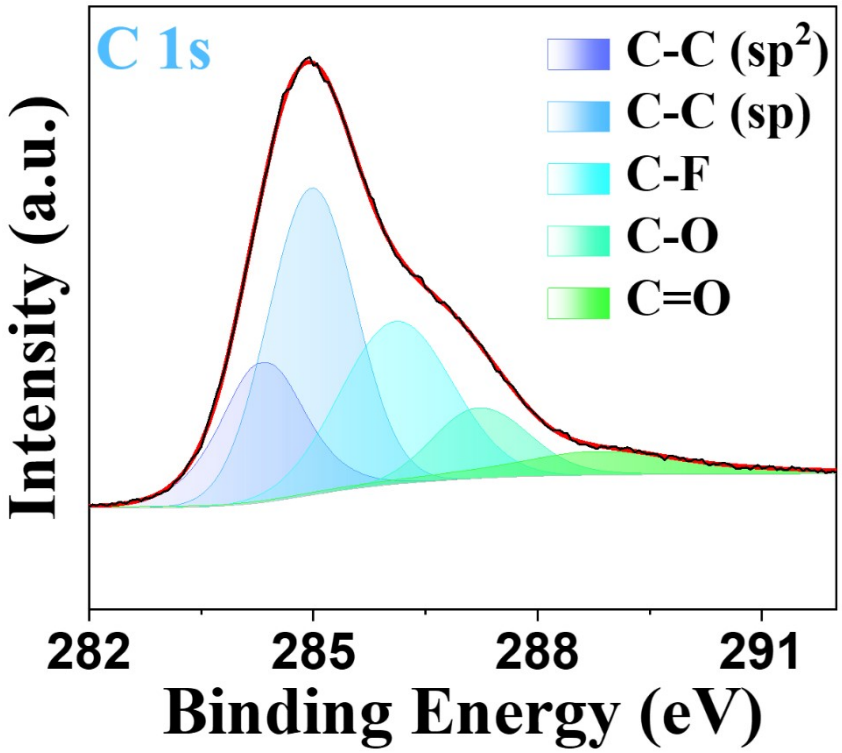

Fig. S5 XPS C1s spectrum of FsGDY.

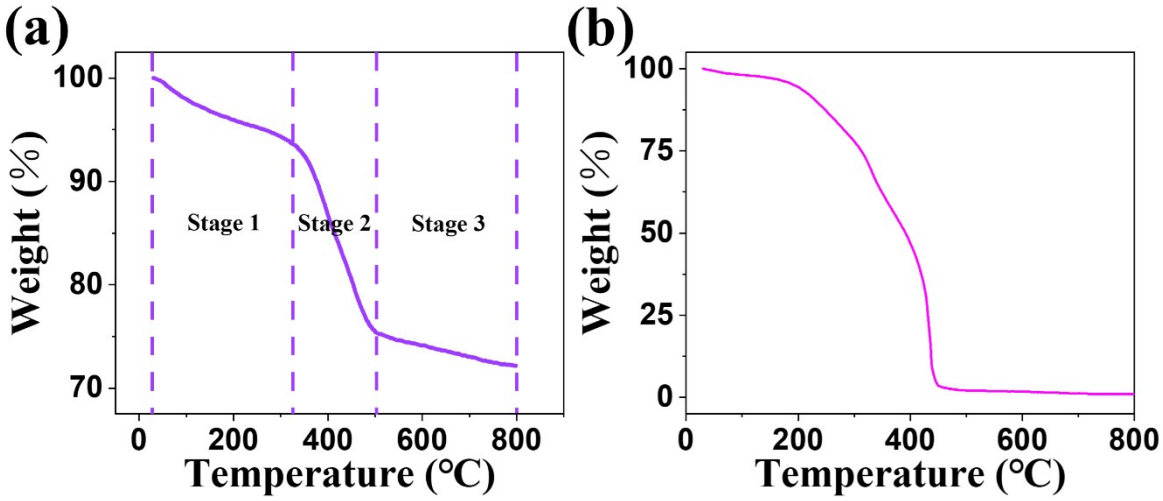

Fig. S6 (a) TG analysis of the FsGDY/Fe_2O_3 composite. (b) TG analysis of the pure GDY.

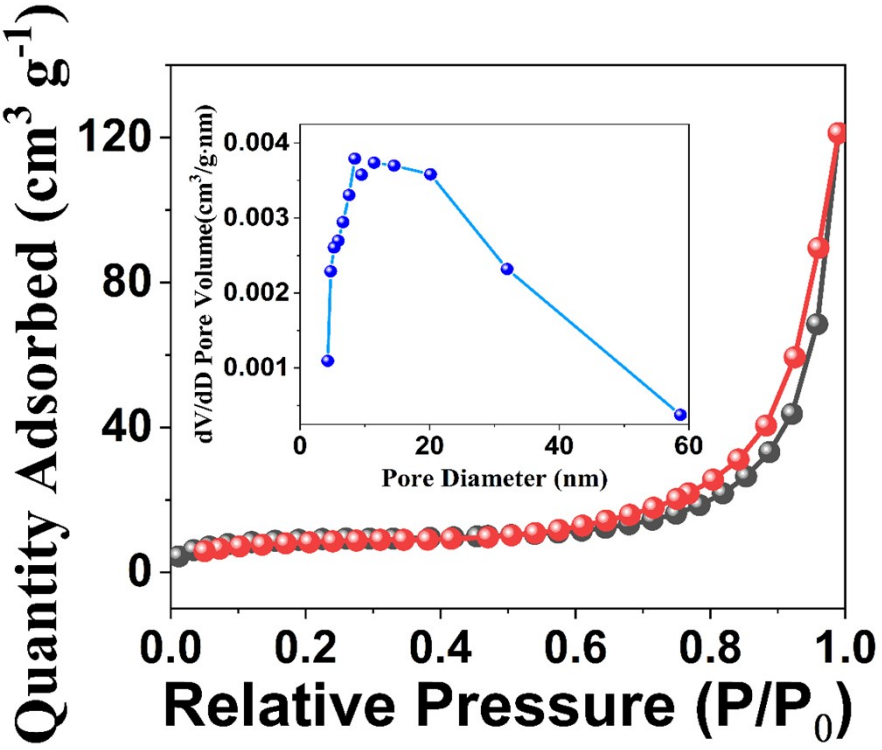

Fig. S7 BET analysis and pore size distribution (inset) of the pure GDY.

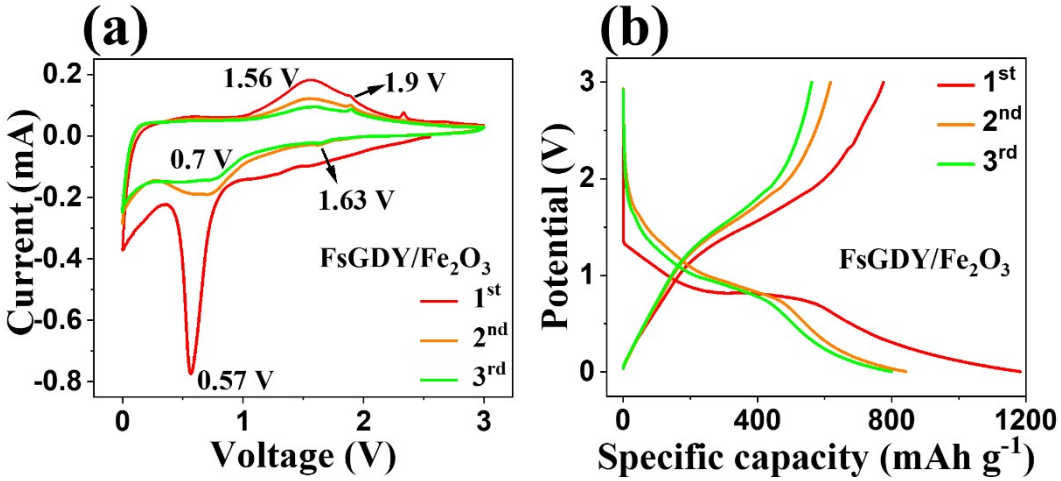

Fig. S8 (a) CV curves of FsGDY/Fe$_2$O$_3$. (b) Galvanostatic charge-discharge curves of FsGDY/Fe$_2$O$_3$.

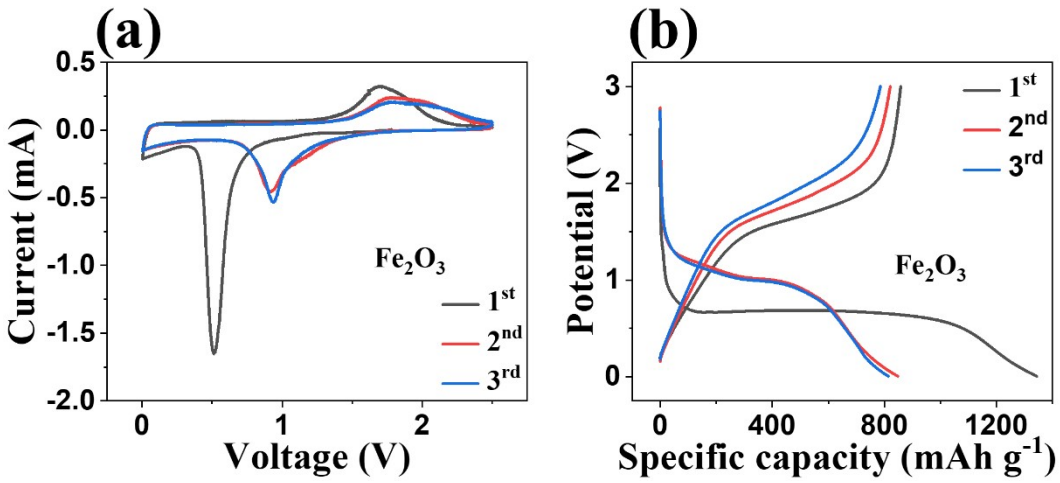

Fig. S9 (a) CV curves of Fe_2O_3. (b) Galvanostatic charge-discharge curves of Fe_2O_3.

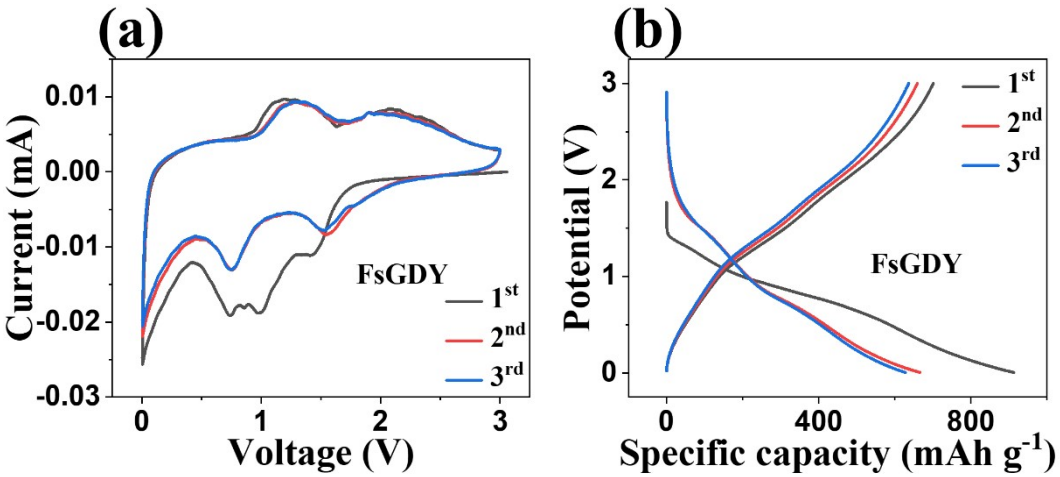

Fig. S10 (a) CV curves of FsGDY. (b) Galvanostatic charge-discharge curves of FsGDY.

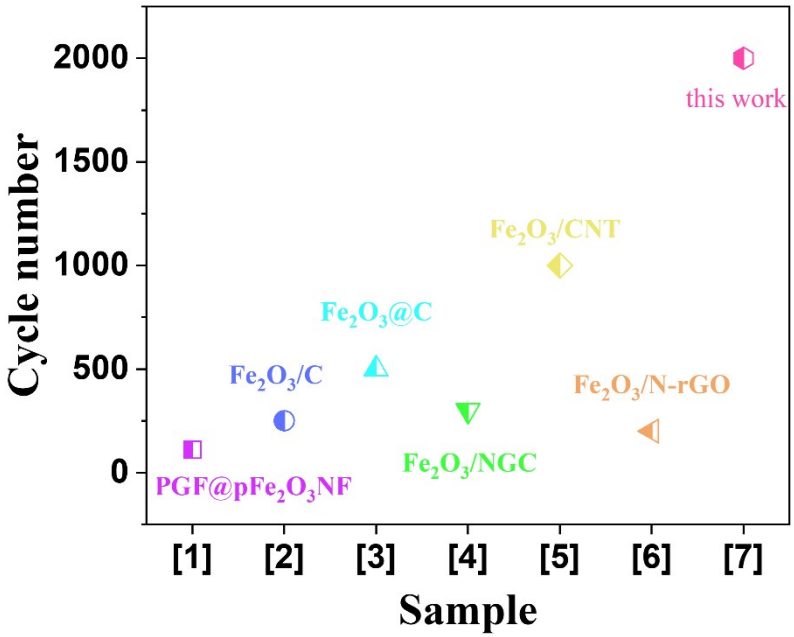

Fig. S11 Comparison of Long-Term Cycling Performance of Fe_2O_3-Based Composites.

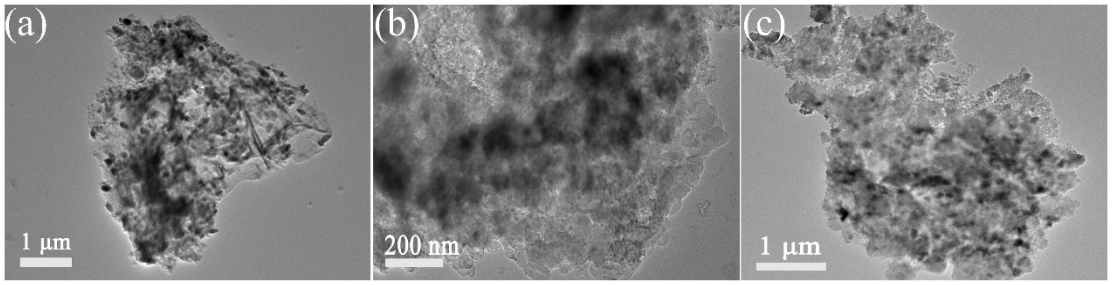

Fig. S12 TEM images of the FsGDY/Fe_2O_3 composite at different charge-discharge voltages. (a) Discharged to 1 V. (b) Discharged to 0.1 V. (c) Charged to 2 V.

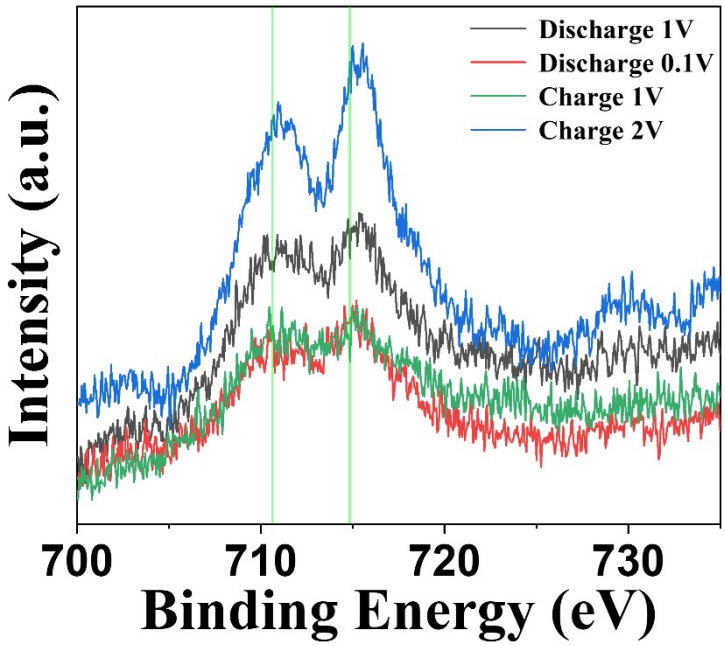

Fig. S13 XPS spectra of Fe at different voltages.

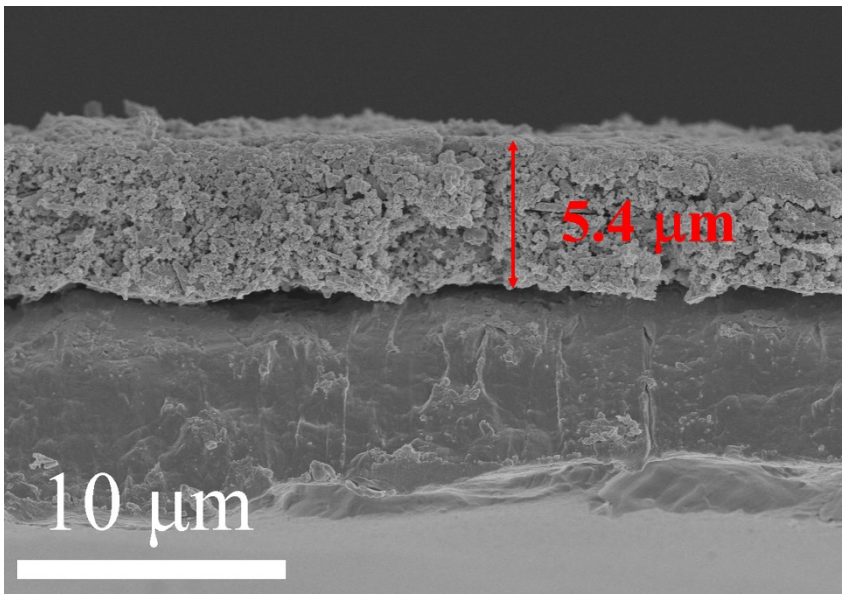

Fig. S14 Thickness of the FsGDY/Fe_2O_3 composite electrode.

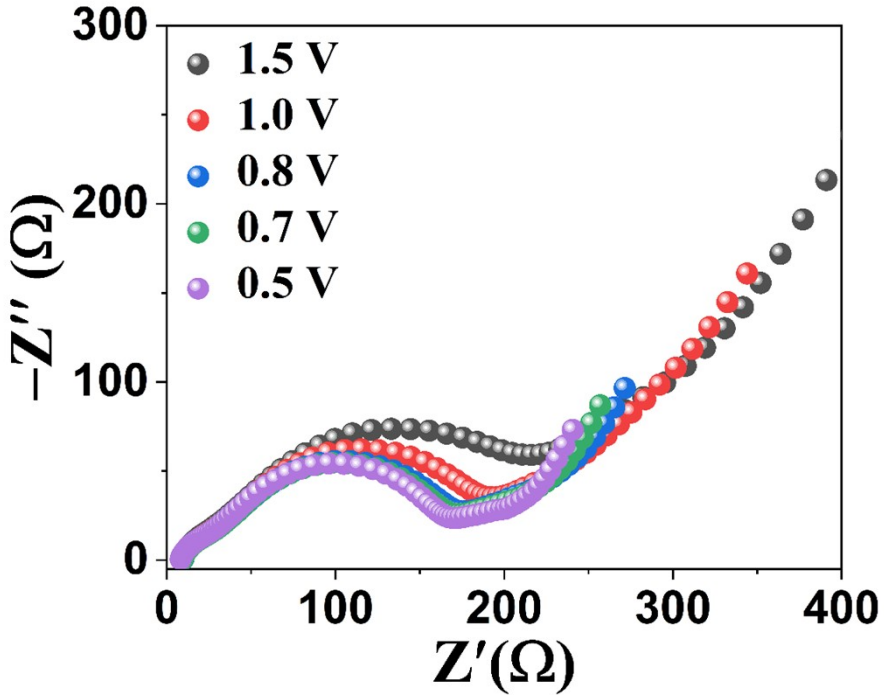

Fig. S15 EIS measured at different voltages.

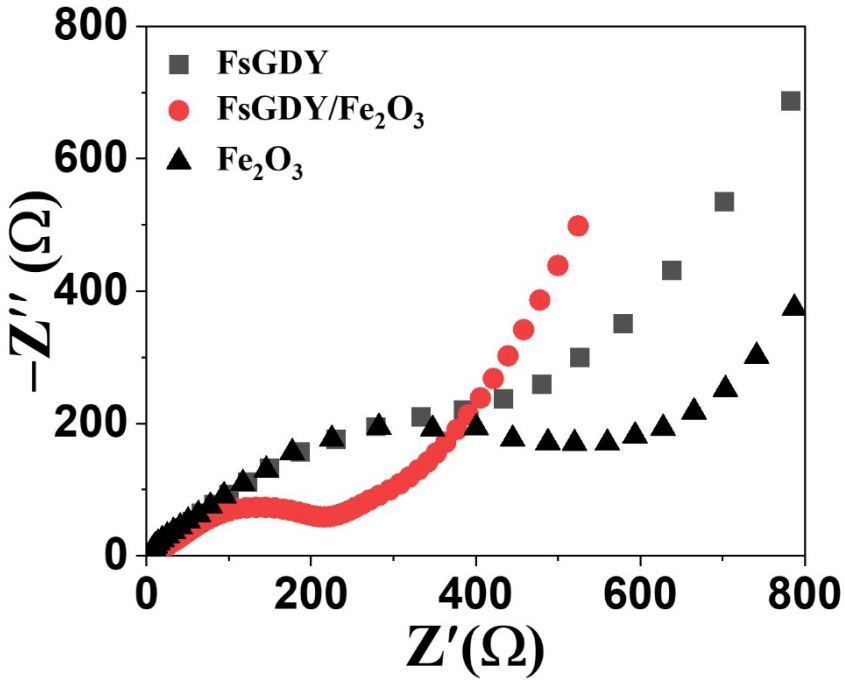

Fig. S16 Comparison of impedance of FsGDY, Fe_2O_3, and FsGDY/Fe_2O_3.

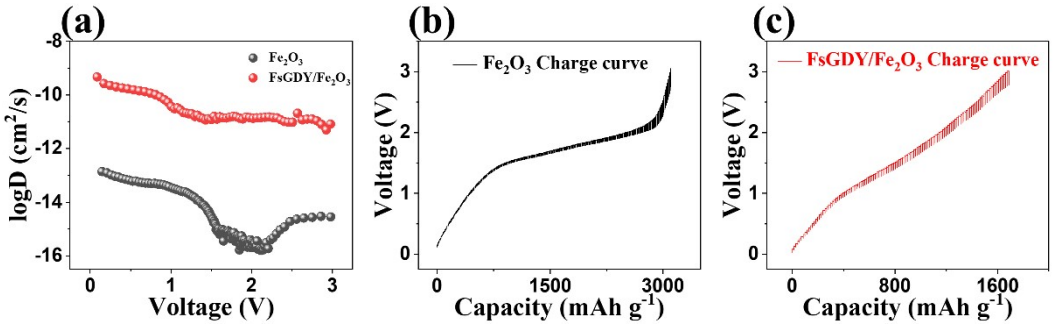

Fig. S17 (a) Comparison of lithium-ion diffusion coefficients (logD) for FsGDY/Fe_2O_3 and pure Fe_2O_3. (b) Voltage–capacity curve of pure Fe_2O_3 during the galvanostatic charging process. (c) Voltage–capacity curve of FsGDY/Fe_2O_3 during the galvanostatic charging process.

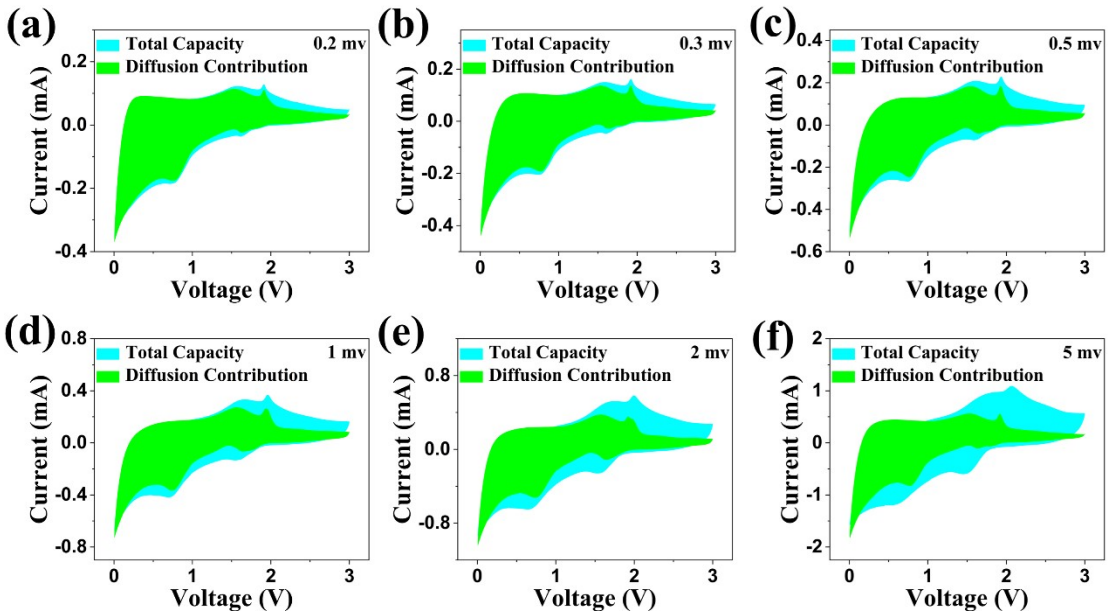

Fig. S18 Diffusion-controlled contribution in the total current of cyclic voltammetry curves at different scan rates.

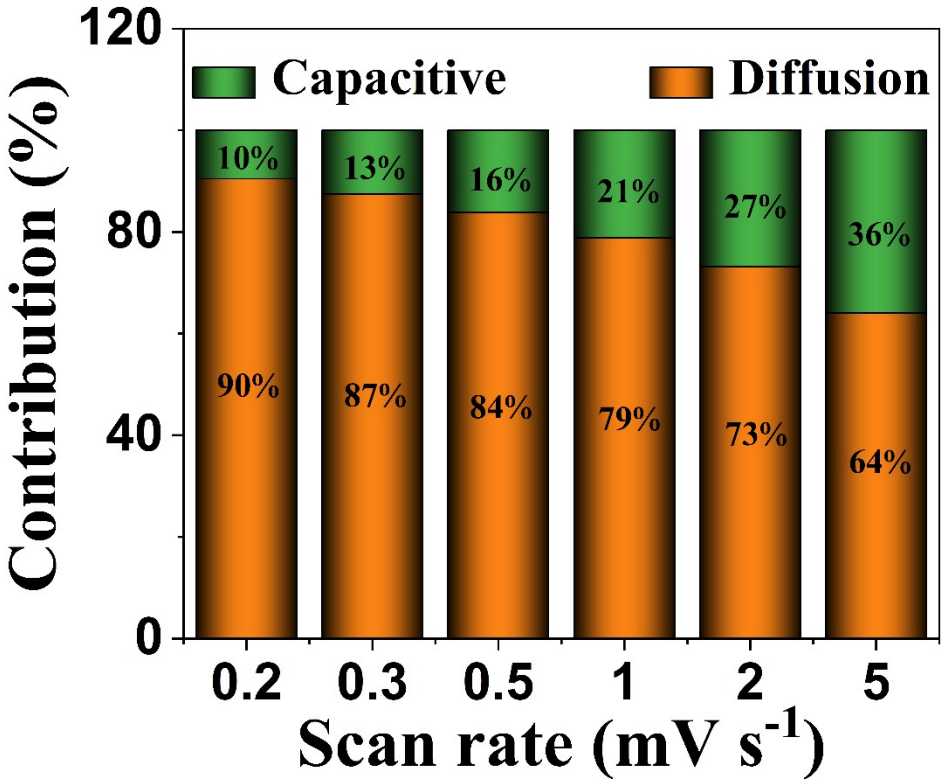

Fig. S19 Capacitive and diffusion-controlled contributions to the total charge storage.

[1] Ma, J.; Kong, Y.; Liu, S. C.; Li, Y. T.; Jiang, J. B.; Zhou, Q. Y.; Huang, Y. S.; Han, S. Flexible Phosphorus-Doped Graphene/Metal-Organic Framework-Derived Porous Fe2O3 Anode for Lithium-Ion Battery. ACS APPLIED ENERGY MATERIALS 2020, 3 (12), 11900-11906.

[2] Hu, J. L.; Wang, Z. Y.; Li, C.; Lan, D. H.; Yi, B.; Tian, Q. H.; Yi, Z. Q. A relatively simple preparation strategy of void-involved Fe2O3/C and its lithium storage. JOURNAL OF ENERGY STORAGE 2025, 109.

[3] Pan, Y. Y.; Luo, C. A.; Yang, D.; Sun, P. K.; Chen, J. Z.; Sui, Z. Y.; Tian, Q. H. Ultrathin porous Fe2O3@C nanosheets: Novel preparation strategy and high lithium storage. APPLIED SURFACE SCIENCE 2023, 635.

[4] Song, J.; Maulana, A. Y.; Kim, H.; Yun, B.; Gim, H.; Jeong, Y.; An, N.; Futalan, C. M.; Kim, J. N-doped graphitic carbon coated Fe2O3 using dopamine as an anode material for sodium-ion batteries. JOURNAL OF ALLOYS AND COMPOUNDS 2022, 921.

[5] Cao, Y.; Zhang, A. Q.; Zhang, H.; Ding, G. Q.; Zhang, L. S. A facile route to achieve Fe2O3 hollow sphere anchored on carbon nanotube for application in lithium-ion battery. INORGANIC CHEMISTRY COMMUNICATIONS 2020, 111.

[6] Huang, Y.; Li, Y. W.; Huang, R. S.; Ji, J. C.; Yao, J. H.; Xiao, S. H. One-pot hydrothermal synthesis of N-rGO supported Fe2O3 nanoparticles as a superior anode material for lithium-ion batteries. SOLID STATE IONICS 2021, 368.